Single-Frequency CW Vertical External Cavity Surface Emitting Semiconductor Laser at 1003 nm and 501nm by Intracavity Frequency Doubling

Mathieu Jacquemet, Manuela Domenech, Gaëlle Lucas-Leclin, Patrick Georges, Jean Dion, Martin Strassner, Isabelle Sagnes, Arnaud Garnache

Single-frequency cw vertical external cavity surface emitting semiconductor laser at 1003 nm and 501 nm by intracavity frequency doubling

M. Jacquemet[1], M. Domenech[1], G. Lucas-Leclin1, P. Georges[1], J. Dion[2],
M. Strassner[2], I. Sagnes[2], A. Garnache[3]

[1] Laboratoire Charles Fabry de l'Institut d'Optique, CNRS, Univ. Paris-Sud,
Campus Polytechnique RD 128, 91127 Palaiseau Cedex, France
[2] Laboratoire de Photonique et de Nanostructures, Route de Nozay CNRS UPR 20,
91460 Marcoussis, France
[3] Centre d'Electronique et de Micro-optoélectronique de Montpellier, CNRS UMR5507,
Universite Montpellier 2, 34095 Montpellier Cedex 5, France

ABSTRACT This work reports single-frequency laser oscillation at $\lambda = 1003.4$ nm of a diode-pumped vertical external cavity surface-emitting semiconductor laser for metrological applications. A low thermal resistance of the semiconductor active component is achieved by solid-liquid interdiffusion bonding onto a SiC substrate. The spectro-temporal dynamics of the laser is theoretically studied. Experimentally, an output power of 1.7 W is demonstrated in free running operation, and up to 500 mW in a true single longitudinal mode. Furthermore, single-frequency laser emission at $\lambda = 501.7$ nm is obtained by intracavity frequency doubling, resulting in a total output power as high as 62 mW.

PACS 42.55.Px; 42.55.Xi; 42.62.Eh; 42.65.Ky

1 Introduction

Indisputably, since the advent of high-power laser diodes, the laser technology is experiencing a fundamental structural change, as this semiconductor device has become the key element of a new breed of laser systems that are competing with gas lasers and lamp-pumped solid-state lasers. Owing to their high power efficiency yield, low cost, compact structure and ease of cooling, high-power lasers are becoming increasingly attractive. In this field, diode-pumped vertical-external-cavity surface emitting lasers (VECSEL's) combine the approaches of diode-pumped solid-state lasers and engineered semiconductor lasers generating both circular diffraction limited output beams, and high average powers [1, 2]. In addition, VECSEL's allow easy scaling of the output power into the multiwatt range, by increasing the laser mode area at higher pump powers, thus maintaining a high beam quality. Furthermore, the external configuration allows other interesting applications like passive mode-locking with a saturable absorber in picosecond [3] to femtosecond [4]

pulse operation, broadband laser absorption spectroscopy [5] or tunable narrow-linewidth operation [6–8]. The ideal materials to fabricate these structures are the III-V compound semiconductors because a large spectrum of laser wavelengths becomes accessible from the blue to the mid-infrared. For applications in the near infrared VECSEL's have most often been grown on GaAs substrates using efficient high contrast GaAs/AlAs reflectors. These devices operate in different wavelength regions: around 850 nm using lattice-matched GaAs/AlGaAs quantum wells [6, 9] and around 1 μm using strained InGaAs/GaAs quantum wells [1–5]. However, the relatively poor thermal conductivity of GaAs (~ 45 W m^{-1} K^{-1}) might prevent efficient heat removal from the active region to an appropriate heatsink, resulting in an excessive heating of the semiconductor structure. This leads to an increase of the threshold pump density as well as a shift of the wavelength of the gain as compared to the Bragg mirror. Two solutions have been mainly described in the literature: first growing the structure upside down and removing the GaAs substrate to dissipate the heat directly through the Bragg mirror [1, 10, 11]; or secondly removing the heat through the top of the semiconductor structure by bonding it to a material of high thermal conductivity and good optical quality [2, 7, 9, 12]. In the second case the choice for that heatspreader is reduced and only solutions using sapphire, diamond or SiC have been reported. In addition, the intracavity optical heatspreader introduces some birefringence, a parasitic Fabry–Pérot etalon effect, thermal lensing and non-negligible optical losses [9, 12]. In this work, we describe the first laser technology using a process based on low thermal AuIn$_2$ bonding onto SiC to improve the heat dissipation in electro–optical devices and hence boost their performances [13].

Furthermore, by frequency-doubling of solid-state lasers emitting at wavelengths around 1 μm, one can reach wavelengths between 498 and 532 nm corresponding to molecular iodine (^{127}I$_2$) hyperfine transitions used in metrological applications such as references for high-resolution spectroscopy [14, 15]. These transitions are numerous and the lower their wavelength the narrower their natural line-

width [16]: with a linewidth as low as 11 kHz, hyperfine transitions around 501.7 nm are obviously of great interest [17]. However no direct optical transition exists in solid-state materials at this wavelength, which is thus only achievable by frequency-doubling of an infrared laser source operating at 1003.4 nm. Yb and Nd-doped crystals or Yb-doped fibers are the actual alternatives proposed as diode-pumped laser mediums in the near infrared [18]. From these sources, only few have a high emission cross-section at 1003.4 nm, the choice for a diode-pumped solid-state laser material thus becomes rather limited [19]. However, VECSEL's may emit at virtually any wavelength depending on the choice of the semiconductor medium, and efficient cw intracavity second-harmonic generation has already been demonstrated [11, 20]. Finally, single-frequency operation of a VECSEL is obtained in very simple and compact laser cavities, thanks to the resonant periodic gain of the semiconductor layer structure that avoids the spatial hole-burning effect. Lastly, for this application we should take advantage of the ultra-low quantum limit of the VECSEL linewidth [8]. Indeed, laser linewidths of around a few kHz have been experimentally demonstrated, which were only limited by acoustic noise and pump fluctuations [6–8].

Therefore, in this work, taking into account the best features of diode-pumped semiconductor lasers and the advantages of laser systems around $1 \mu m$, a simple scheme for single-frequency laser oscillation at 1003 nm of a diode-pumped external-cavity surface-emitting semiconductor laser fabricated by the MOCVD epitaxy technique on GaAs substrate is proposed. An output power of up to 500 mW in a single transverse and longitudinal mode has been obtained, as well as the main VECSEL features. In addition, intracavity second harmonic generation at 501.7 nm using a $KNbO_3$ crystal with an output blue-green power of 62 mW is also reported.

2   Gain structure design and fabrication

The $\lambda_L = 1010$ nm half-VCSEL designed for $\lambda_p = 808$ nm pumping used in the present work was grown by MOCVD using TMGa, TMAl, TMIn, and AsH_3 at 60 mTorr and at a temperature of 650 °C [13]. The multilayer mirror at the top of the GaAs(100) substrate, which serves as one of the resonator mirrors, is obtained by using 27.5 pairs of GaAs/AlAs. Grown on top of the Bragg mirror is a 3.75λ thick cavity with $N_{QW} = 5$ compressively strained $L_{QW} = 7$ nm $In_{0.2}Ga_{0.8}As$/GaAs quantum wells (QW's) distributed among the seven optical standing-wave antinode positions with a distribution function 1-1-1-0-1-0-1 (starting from the surface, see Fig. 1) such as the carrier density remains almost equal in all QW's. The number of QW's was optimised to obtain a low laser threshold and a large enough differential gain at 300 K, with about 1%–1.5% of total optical cavity losses [21]. The choice of a low number of QW's, as compared to other published designs, avoids the need to grow strain-compensating layers between the QW's [1] and results in a very low transparency threshold. The calculated pump absorption at $\lambda_p = 808$ nm is nearly 70% in the $1 \mu m$ thick barrier layers; still this reduced absorption limits the overall efficiency of our structure. On top of the gain region, a 30 nm AlAs confinement layer and an 8 nm capping layer of GaAs were added [4]. The structure was grown in reverse order.
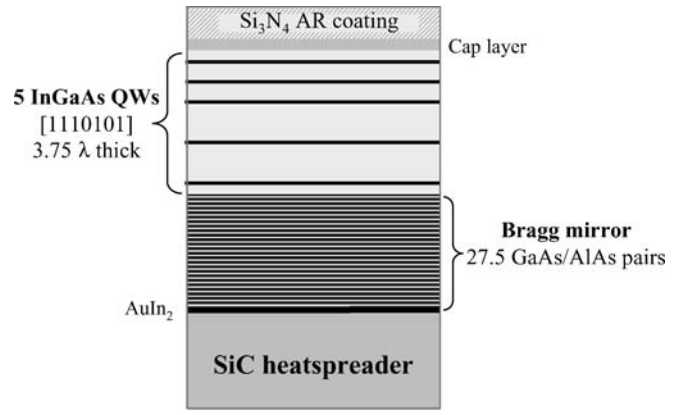
FIGURE 1   Semiconductor layer structure of the active medium and Bragg grating, onto the SiC heatspreader, forming the 1/2-VCSEL
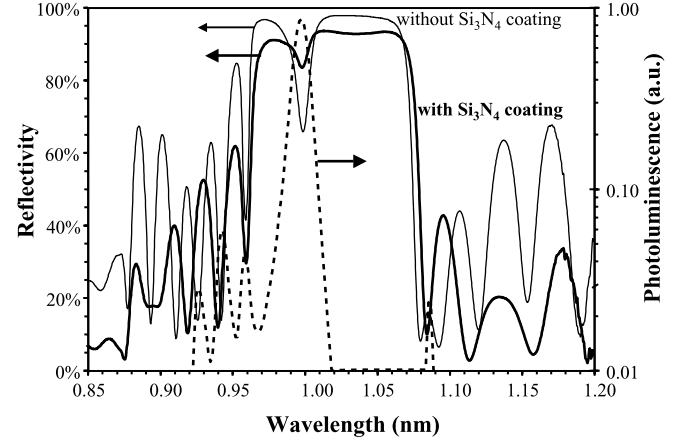
FIGURE 2   Reflectivity of the 1/2-VCSEL bonded onto the SiC substrate (left; *black curve*: with AR coating, *grey curve*: without AR coating) and photoluminescence spectrum (*dotted line*, right) under low-power excitation before the AR coating deposition. The etalon effect of the 1/2-VCSEL is visible on the reflectivity spectrum before AR coating around $1.0 \mu m$

To improve the heat dissipation, the 1/2-VCSEL was bonded onto a $280 \mu m$ thick Si substrate (thermal conductivity of $\kappa_{s1} = 150$ W m^{-1} K^{-1}) or a $270 \mu m$ thick SiC substrate (thermal conductivity of $\kappa_{s2} = 490$ W m^{-1} K^{-1})on the Bragg mirror side by solid–liquid inter-diffusion (SLID) bonding with $AuIn_2$ [13, 22]. The $AuIn_2$ bonding is formed at 200 °C, but its fusion temperature is 490 °C; this allows further processing steps at elevated temperatures and does not induce any strain-related degradation of the optical properties of the structure. Then both mechanical polishing and wet selective etching was utilised to remove the GaAs substrate. Finally, a Si_3N_4 anti-reflection coating was deposited by the means of plasma enhanced chemical vapour phase deposition (PECVD) at high temperature (300 °C) to protect the top surface from oxidation and to weaken the residual etalon resonances of the semiconductor structure. Photoluminescence measurements of the QW's have been carried out before and after the bonding procedure, with it being possible to conclude that the $AuIn_2$ bonding technique does not modify the optical properties of QW's. The reflectivity and photoluminescence spectra of the bonded structure are shown in Fig. 2, demonstrating an optimised design with a good matching between the central wavelength of the Bragg mirror and the QW gain

for 300 K operation. With a residual air-structure interface reflection of about 6%, the fraction of incident pump power absorbed in the active region is evaluated to $A_p = 66\%$. The remaining pump power is absorbed in the GaAs layers of the Bragg mirror.

3 Theoretical and experimental thermal properties of the 1/2 VCSEL

The heat diffusion in the whole semiconductor structure has been theoretically studied assuming a perfect metal bonding between the Bragg mirror and the various substrates. The pump absorption was supposed to decrease exponentially through the active region and the Bragg mirror; the pump beam transverse profile was top-hat. We have evaluated the average thermal resistance R_{th} of the 1/2-VCSELs over the laser beam area, measured between the top surface of the Peltier cooler and the QW's. The values of R_{th} are given relatively to the incident pump power. Assuming an internal quantum efficiency η_i of 80% for the QW's and of 10% for the GaAs in the Bragg mirror, the fraction of the incident pump power converted to heat was calculated to be 50%.

We implemented an analytical three-layer model (active region/substrate/copper block), in which the substrate itself is perfectly bonded onto an infinite copper block (thermal conductivity of 400 W m^{-1} K^{-1}) [23]. The active region consists of the QW's and the Bragg mirror layers, with a total thickness $e_v = 5.45\ \mu m$. We chose a mean value of $\kappa_v = 32$ W m^{-1} K^{-1} as its thermal conductivity for the calculations presented on Fig. 3. We have evaluated that for pump beam waist radii larger than the critical value $r_c = e_v(\kappa_s/\kappa_v)$, the major contribution to the temperature increase in the QW layers arises from the substrate. Then the heat flow in the 1/2-VCSEL is purely 1D, and the temperature rise only depends on the pump power density. These critical pump radii are $r_c = 7.7\ \mu m$, $25.5\ \mu m$ and $83.4\ \mu m$ for the GaAs, Si and SiC substrates respectively.

Furthermore, the thermal resistance has been evaluated with a finite-element numerical simulation (FEMLAB). A 10 mm lateral width of the sample was considered. Furthermore, a 50 μm thick heat-paste layer (thermal conductivity of 2 W m^{-1} K^{-1}) embedded between the substrate and the copper block has been taken into account. The thermal resistances evaluated from both the numerical and the analytical models are compared in Fig. 3. The analytical model, which mainly neglects the heat-paste layer contribution, underestimates the thermal resistance from 2 to 30% in the range of pump radii investigated here (30–350 μm).
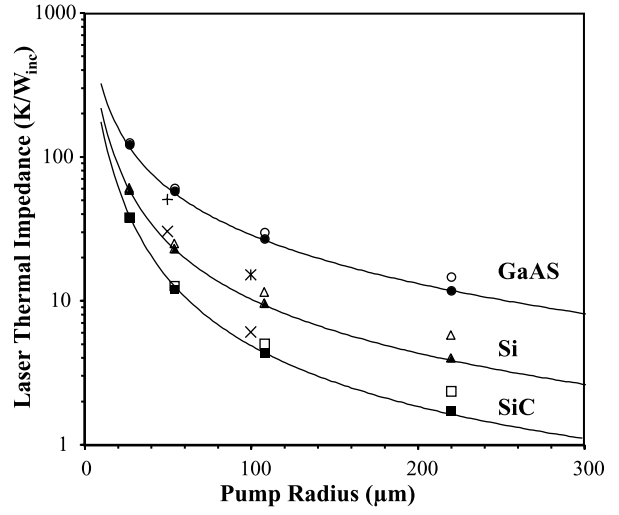

FIGURE 3 Comparison of the analytical (*lines*) and numerical (*full marks*: without heatpaste; *empty marks*: with 50 μm thick heatpaste) simulations of the thermal resistance of three 1/2-VCSEL structures on respectively SiC ($e_S = 270\ \mu m$ – squares), Si ($e_S = 280\ \mu m$ – *triangles*) and GaAs ($e_S = 350\ \mu m$ – *circles*) substrates, vs the pump radius. Experimental evaluations of the thermal resistance deduced from the shift of the emission wavelength are added (GaAs +, Si ∗, SiC×)

These simulations have been compared to the experimental evaluation of the thermal resistance of our three samples under laser operation close to threshold, through the measurement of the shift of the emission wavelength – i.e. of the QW's gain maximum as the AR coating avoids any Fabry–Pérot effect – with the incident pump power and the heatsink temperature. For a pump waist radius $W_p = 100\ \mu m$, a thermal resistance of 6 K/W_{inc} was measured for the structure bonded onto SiC, which is in relatively good accordance with the theoretical value of 5.6 K/W_{inc}. Under the same experimental conditions, the structure onto the Si substrate had a thermal resistance of about 15 K/W_{inc}, slightly higher than the 11.5 K/W_{inc} theoretical evaluation. For comparison the experimental thermal resistance of the 1/2 VCSEL on GaAs was about 50 K/W_{inc} for $W_p = 50\ \mu m$ (Fig. 3). The agreement between theory and experiment shows the high quality of the metal bonding process. The significant reduction of the thermal resistance of the bonded structures was further corroborated by the fact that, under laser operation, the output power of the 1/2-VCSEL on SiC was only limited by the available pump power for a pump waist radius of 100 μm and the experimental set-up described in Sect. 4 (Fig. 6). On the contrary with the structure on GaAs, no laser operation was achieved under the same cavity and pump conditions, and the max-
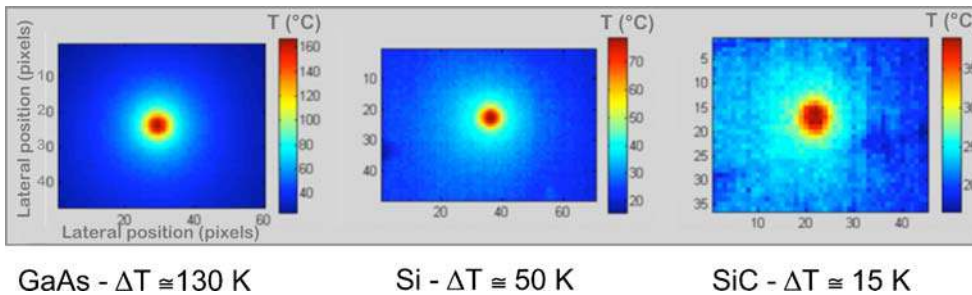
FIGURE 4 Temperature maps of the 1/2-VCSEL structures under optical pumping ($\lambda = 808$ nm, $P_p = 4$ W, $W_p = 250\ \mu m$) without laser operation

GaAs - $\Delta T \cong 130$ K   Si - $\Delta T \cong 50$ K   SiC - $\Delta T \cong 15$ K

3
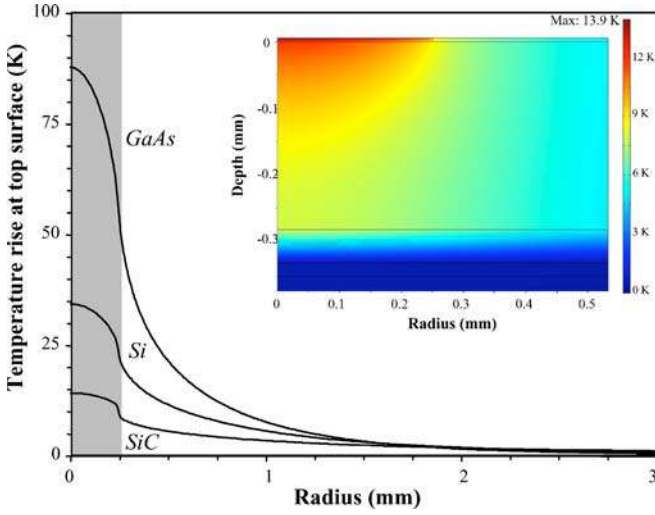
FIGURE 5 Theoretical temperature distributions at the top surface of the 1/2-VCSEL devices under optical pumping ($\lambda = 808$ nm, $P_p = 4$ W, $W_p = 250\,\mu$m) without laser operation (thermal load = 75%); a 50 μm-thick heatpaste layer between the copper and the substrate is considered. *Inset*: Temperature distribution inside the device through the various layers for the structure on SiC
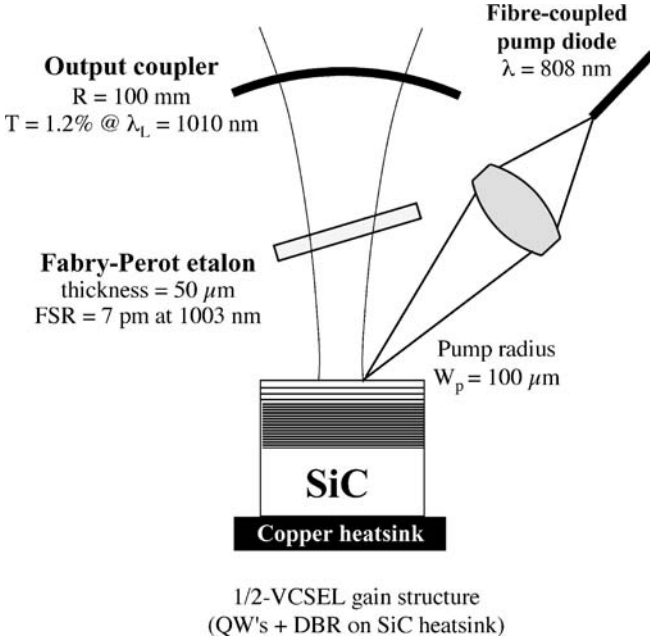
FIGURE 6 Experimental set-up for high-power laser emission in the infrared

imum output power was only 100 mW for a pump waist radius of 50 μm. With the structure bonded onto Si and a 100 μm pump waist radius, an output power of 510 mW was obtained for an incident pump power of 3.5 W but it remained limited by the thermal roll-over at higher pump powers (Fig. 7).

In addition, the temperature at the top surface of the 1/2-VCSELs has been experimentally measured under continuous wave (cw) optical pumping, in the spontaneous emission regime (without any laser cavity), with the help of an infrared camera operating in the 8–12 μm range [25]. The lateral resolution of the mapping was 60 μm, thus only suitable for large pump beam waists. With a maximum temperature rise limited to 15 K for a 4 W pump beam focused on a 250 μm

radius waist, the structure bonded onto SiC obviously demonstrated the lower thermal resistance (Fig. 4). Moreover, the surface homogeneity of our bonded components is obvious from these pictures. Finally there is a good qualitative agreement between these measurements and the theoretical predictions under the same conditions (see Fig. 5); the largest deviation from theory is observed with the 1/2-VCSEL on GaAs, which we attribute to the fact that in that case the temperature measurement integrates the whole depth of the device due to the transparency of GaAs in the 8–12 μm spectral range, whereas the opacity of the AuIn$_2$ bonding layer ensures that the temperature is measured in the active zone only.

4 High power laser characterisation

With the aim of producing high powers around 1 μm, we naturally focused our experimental work on the 1/2-VCSELs structures bonded onto Si and SiC substrates. The VECSEL system was set up in a simple and compact cavity configuration as shown on Fig. 6. The 1/2-VCSEL was mounted onto a copper heatsink to control the temperature of the device with a Peltier module. The semiconductor structure was pumped with a cw fiber-coupled $\lambda_p = 808$ nm laser diode delivering up to 7 W focused on approximately a 100 μm radius spot with an incidence angle of 20°. The external cavity was simply formed by the 1/2-VCSEL and a concave dielectric mirror with a reflectivity of $R_{oc} = 98.8\%$ at $\lambda_L = 1010$ nm and a curvature radius of 100 mm. The overall cavity length was around $L_c = 95$ mm, leading to a cavity free-spectral-range (FSR) of ~ 5 pm. For both 1/2-VCSEL bonded onto Si and SiC, the incident pump power at threshold was 0.8 W in cw operation at 283 K, corresponding to an incident pump power density of $I_{inc}^{th} = 2.2$ kW/cm^2. Note that this threshold is particularly low as a consequence of our active layer design with few QW's. With the SiC-bonded 1/2-VCSEL, the output power reached 1.7 W at the maximum incident pump power of 7 W and the cw slope efficiency was about 32% (Fig. 7). The beam quality factor M^2 relating the spatial beam properties to an ideal Gaussian beam was found to be < 1.3 at the highest pump power. The linear polarisation of the laser beam was aligned along the [110] semiconductor crystal axis, due to a slight gain dichroism between [110] and [1 − 10] crystal axis. In the compact two-mirror cavity used here, and without any intracavity element, laser oscillation occurred around 1009 nm for the maximum pump power and a heatsink temperature of 283 K. The cw spectral bandwidth was nearly 2 nm, probably broadened by the QW's gain jitter induced by the pump power fluctuations. With the Si-bonded structure, a maximum output power of only 0.5 W was obtained, limited by thermal roll-over. This is due to its higher thermal resistance as described previously.

These experimental results on the SiC structure are in good agreement with the theoretical evaluation of the VECSEL behaviour based on (1)–(4) below. Equations (1) and (2) respectively set the relation linking the incident pump power density I_{inc} to the current density per QW $J_{current}$ (in A/cm^2), and the material gain at threshold g_{th} to the cavity parameters. The values for g_0 (1200 cm^{-1}) and J_{tr} (50 A/cm^2), which make the connection between the maximal material gain and the current density per QW, are deduced from [21]

for InGaAs/GaAs quantum wells. $A_p = 66\%$ is the absorption of the incident pump power in the active region. The longitudinal confinement factor Γ_c is 2 and we assumed intracavity losses of $T_i = 0.1\%$–0.2%.

$$I_{inc} = J_{current} \frac{N_{QW}hc}{\lambda_p A_p e} \tag{1}$$

$$g_{th} = g_0 \ln \frac{J_{current}^{th}}{J_{tr}} \approx \frac{T_i + (1 - R_{oc})}{2\Gamma_c N_{QW} L_{QW}} . \tag{2}$$

From these equations, an incident pump power density at threshold I_{inc}^{th} of 1.7 kW/cm² is expected for cw operation at the heatsink temperature of 283 K. The external quantum efficiency η_e, assuming a pump-to-laser beam recovering integral close to unity, is given by

$$\eta_e \approx \eta_i \frac{\lambda_p}{\lambda_L} A_p \times \frac{1 - R_{oc}}{(1 - R_{oc}) + T_i} , \tag{3}$$

and finally the laser output power is expressed as

$$P_{out} = \eta_e \left(I_{inc} - I_{inc}^{th}(T) \right) \times \pi W_p^2 . \tag{4}$$

In (4) the evolution of the laser threshold pump density I_{inc}^{th} with the QW's temperature T is theoretically taken into account through the characteristic temperature T_0, evaluated to 60 K in these experiments [21]. T is a function of the incident pump power and of the thermal resistance of the device, for which the experimental values have been considered in the theoretical plots in Fig. 7. This figure shows the very good agreement between the theoretical evaluation of the output power with the incident pump power, and our experimental results. An output power limited to 1.8 W is predicted for an incident pump power of 7.9 W and a 100 μm radius pump waist. Moreover, we have theoretically checked that the experimental pump waist is very close to the optimal one (105 μm) for maximum laser power emission at an incident pump power of 7 W. Finally, these simulations have been used to estimate the maximum output power which could be extracted

from our three 1/2-VCSELs at the heatsink temperature of 283 K, with cavity specifications similar to the experimental ones; the thermal resistances were calculated from our numerical model assuming a perfect bonding between the copper heatsink and the substrate (see Sect. 3 and Fig. 3). The incident pump power value was optimised for each structure such that it leads to the maximum extracted power (Fig. 7). Obviously the low thermal conductivity of GaAs limits the emitted laser power to 0.1 W at the optimised pump beam waist radius W_p of 38 μm. Moreover, no laser effect could be expected with the 1/2-VCSEL on GaAs for $W_p = 100$ μm, in agreement with our experimental observations. On the contrary with the SiC-bonded 1/2-VCSEL, the highest output power should be 6.7 W and would be obtained with a 30 W incident pump beam focused onto a 260 μm radius pump waist.

These results have been compared with the performances that could be expected from the same active gain design but with another thermal management method, such as the top heatspreader [2, 9]. We have modeled the laser operation of our 1/2-VCSEL on GaAs with a 270 μm thick SiC layer optically bonded to its top surface, taking into account a 50 μm thick heatpaste layer between the GaAs substrate and the temperature-stabilised copper mount. Under cw pumping on a waist radius $W_p = 100$ μm, the top heatspreader would allow a significant reduction of the thermal resistance of the device down to 3.7 K/W_{inc}. Thus the output power would grow up to 3.3 W for an incident pump power of 13 W in the same experimental conditions of the Fig. 7. It is valuable to notice that these calculations, presented in Fig. 8, do not take into account the increased losses resulting from the intracavity element. However the advantage of the top heatspreader as compared to the high-conductivity substrate reduces when it goes to higher pump waist radius for high power emission, and the thermal resistances of both designs are similar with $W_p = 250$ μm. Actually the main limitation to the thermal resistance arises form the heatpaste layer in both cases ... The best way to increase the laser output power would be then to increase the number of QW's, to reduce the cavity losses or to profit of a resonant structure in order to increase the T_0 characteristic temperature.
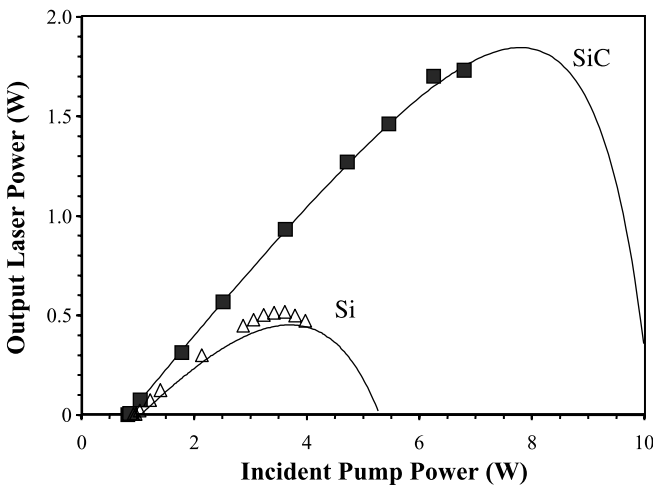
FIGURE 7 Experimental output laser emission from the structures bonded onto SiC (*squares*) and onto Si (*triangles*) in the same conditions ($T = 283$ K, $W_p = 100$ μm); theoretical evolution of the output power vs. the pump for both structures, the parameters are given in the text (*line*)
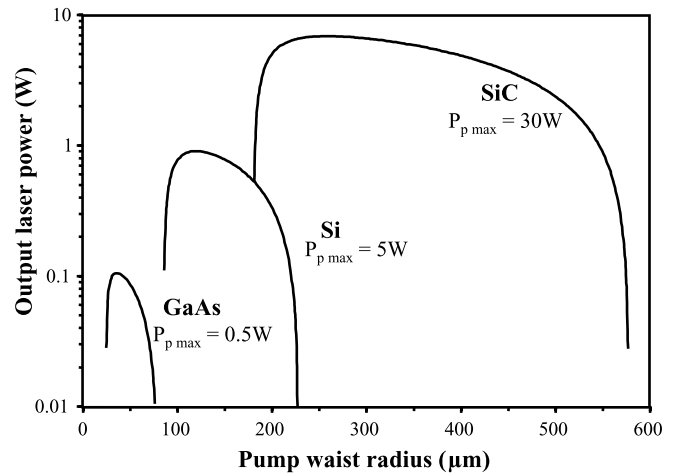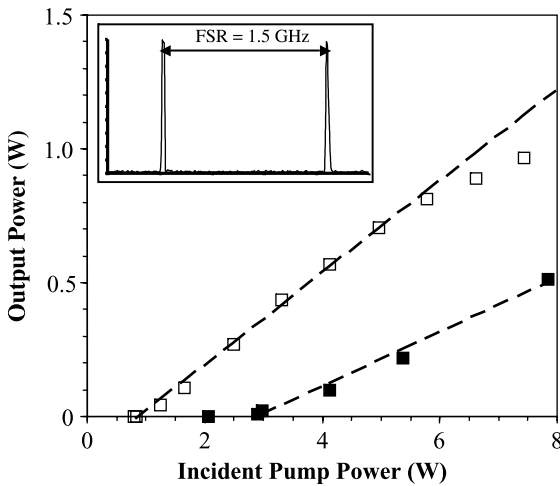

FIGURE 8 Theoretical optimisation of the output laser power vs. the pump waist radius for the three 1/2-VCSELs; the incident pump power is set for maximum laser emission of each structure; the theoretical dependency of the thermal resistances with the pump waist are considered

5   Single-frequency laser operation in the infrared

In order to obtain a stable single-mode laser operation at the desired wavelength of 1003 nm with the SiC-bonded structure, a solid 50 μm thick uncoated glass etalon, with a high FSR of 2 THz ($\Delta\lambda \sim 7$ nm @ 1003 nm) as compared to the QW's gain bandwidth ($\Gamma_g \sim 34$ nm FWHM [21]), was inserted in the cavity. The emission wavelength was tunable from ~ 998 nm to ~ 1010 nm by rotating the etalon and changing the pump position on the 1/2-VCSEL structure, with a maximum output power of 1.3 W at 1006.5 nm (Fig. 9). On the entire incident pump power range the emission wavelength remains strongly controlled by the etalon with a spectral shift less than 0.2 nm. The reduction of the output power by about 30% is due to the additional losses introduced by the solid etalon, which are evaluated to 1.2% from the slope efficiency.

A true single-frequency operation at 1003 nm was obtained for a maximum output power of 0.5 W, which corresponds, to our best knowledge, to the highest single-frequency operation of a diode-pumped VECSEL. The further decrease of the output power can be mainly attributed to the alignments of the cavity and the etalon to force a stable single-frequency laser line, corresponding to extra 1.8% losses. The single-frequency laser spectrum was analysed with a 50 mm confocal scanning Fabry–Pérot interferometer with a FSR of around 1.5 GHz (see inset in Fig. 9). The side-mode suppression ratio was at least 20 dB, but the scanning Fabry–Pérot apparatus function limits the measurement of the laser linewidth. However in this configuration, the laser linewidth should be limited by acoustic and/or thermal noise at the kHz level [7, 8]. No stabilisation of the laser frequency has been carried out.

In order to understand how to stabilise the single-frequency operation of VECSEL, the spectro-temporal laser dynamics have been theoretically studied. Although at the very beginning of the laser operation, several thousands of longitudinal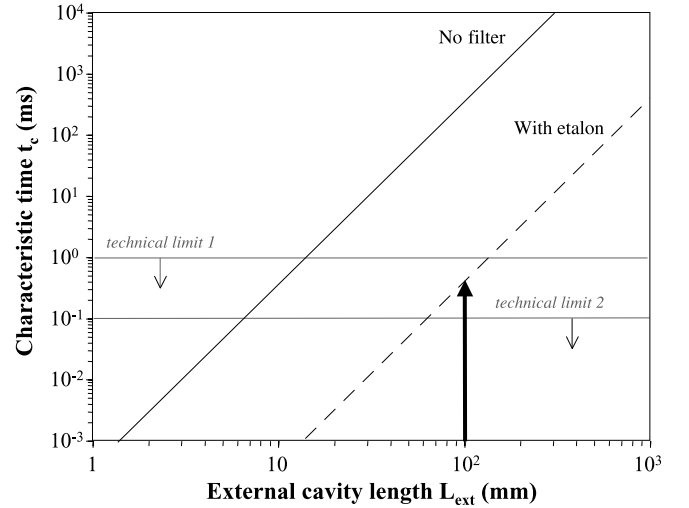 cavity modes are amplified by the gain medium, the laser collapses to a single mode operation after a characteristic time t_c. However if any process disturbs the laser dynamics (gain or mirror jitter, thermal fluctuations ...) before t_c, the emission remains spectrally multimode in cw operation. It has recently been demonstrated both theoretically and experimentally that a single-frequency operation is achievable in a short cavity ($L_c < 100$ mm) VECSEL without any intracavity filter, thanks to their ideal multimode homogeneous gain and the fact that non-linear mode coupling is negligible [8, 24]. In quasi-cw operation, for an ideal homogeneous gain laser, the non-stationary laser bandwidth Δ_L is given by

$$\Delta_L = \Gamma_{g,f} \sqrt{\frac{\ln 2}{\gamma_0 t_g}} \,, \tag{5}$$

where t_g is the generation time elapsed since the beginning of the laser emission, γ_0 is the broadband cavity loss rate (proportional to $1/L_c$; $\gamma_0 = 22.1 \times 10^6$ s^{-1} in our operating conditions with resonator losses $T_i = 1.3\%$), and $\Gamma_{g,f}$ is the gain or filter bandwidth, depending on the intracavity elements [5]. From the expression of the laser bandwidth Δ_L, we have evaluated the characteristic time t_c necessary to achieve a single-mode laser operation after a strong perturbation arises (100% gain modulation e.g.). It is equal to the time t_g within which Δ_L is equal to one FSR of the laser cavity :

$$t_c = \ln 2 \frac{\Gamma_{g,f}^2}{\text{FSR}^2 \gamma_0} = \frac{4 \ln 2}{c \lambda_L^4} \frac{L_c^3 \Gamma_{g,f}^2}{T_i + (1 - R_{oc})} \,. \tag{6}$$

The single-mode characteristic time t_c is plotted in Fig. 9 as a function of the cavity length, with ($\Gamma_f = 1.1$ nm FWHM – parabolic fit) and without ($\Gamma_g = 34$ nm) the 50 μm Fabry–Perot etalon inserted. Experimentally, without the etalon filter

FIGURE 9   cw laser output power vs the incident pump power with the intracavity 50 μm thick solid etalon for the structure bonded onto SiC; *open squares*: narrow spectrum laser emission at 1003 nm; *full squares*: true single-frequency operation at 1003 nm. *Inset*: Scanning Fabry–Pérot trace for the emission at 1003 nm demonstrating single-frequency operation; the 1/2-VCSEL temperature is 283 K

FIGURE 10   Characteristic generation time t_c for the ideal homogeneous QW laser to collapse to single mode operation (simulation), with and without a 50 μm thick glass etalon filter in the cavity. Non-linear mode coupling is neglected. The total losses in the cavity are 1.4%. The typical technical laser width limit, due to acoustic or/and thermal noise in the optical cavity, is depicted by *dot line* #1. *Dot line* #2 shows the lower technical laser width limit due to pump fluctuations for a multimode laser diode pumping. The *black arrow* shows the cavity length used in the experiment

inside the laser cavity, the laser emission was not single-mode and the cw (stationary) laser bandwidth Δ_L covered several hundreds of cavity modes. From (5) it corresponds to a generation time of about 100 µs, i.e. the duration needed for the laser spectrum to narrow its linewidth into a single mode before a perturbation arises. It is one order of magnitude shorter than the typical characteristic time of acoustic or/and thermal noise, which is in the millisecond range [7, 8]. Consequently we believe that the multimode nature of the fibre-coupled pump laser diode generates strong pump intensity fluctuations on a time scale shorter than 100 µs, which in turn destabilise the central wavelength of the gain spectrum and interrupts the spectral narrowing of the VECSEL. From the simulations in Fig. 10 it is obvious that even an etalon with a FSR covering numerous longitudinal modes helps to reduce the characteristic time of the single-mode operation below the typical fluctuations time of the set-up induced by acoustic, thermal noise and/or pump-induced gain fluctuations. It thus allows obtaining of a strong single-mode operation, as observed experimentally.

6 Intracavity second harmonic generation at 501.7 nm

For intracavity second harmonic generation (SHG) at 501.7 nm, we used a four-mirror Z-cavity with a total length of around 630 mm (Fig. 11). The mirrors M_1 and M_2 had a radius of curvature of 200 mm, and a reflectivity higher than 99.98% in the range 900–1100 nm. M_3 was a 75 mm spherical mirror with a reflectivity > 99.9% in the range 650–1100 nm. The laser cavity had two different outputs with similar powers at 501.7 nm because of the high transmission of all the mirrors in the visible range. We chose KNbO$_3$ as the non-linear crystal for its high non-linear coefficient ($d_{\text{eff}} = 9$ pm/V), and the fact that non-critical type I phase-matching is achieved at the temperature of 75.6 °C. The KNbO$_3$ crystal was b-cut, 9.5 mm long and anti-reflection coated for both fundamental and second harmonic wavelengths. The waist radius inside the crystal was evaluated to about 90 µm. A two-quartz-plate Lyot filter and a 100 µm thick FP etalon were also inserted, not only to select the desire emission wavelength, but also to obtain a stable single frequency operation, which was impossible to achieve without the etalon. The crystal was temperature-regulated in an oven, and oriented such that the intracavity fundamental laser beam at 1003.4 nm was polarised along its a-axis, while the second-harmonic generated beam was polarised along its c-axis.

Figure 12 represents the single-frequency output power of the green-blue emission as function of the incident pump power at 808 nm. A total maximum cw output power of 62 mW at 501.7 nm in two beams for a 6.5 W pump power was obtained. The infrared intracavity power was estimated via the residual transmission of mirror M_3 at 1 µm to be about 10 W; this leads to a second harmonic generation conversion efficiency of only 0.6%. This low conversion efficiency is attributed to the constraints imposed by the dimensions of the crystal oven, leading to a rather large waist inside the crystal and a confocal parameter much longer (~ 115 mm) than the crystal length [19]. Moreover, the residual losses introduced by the intracavity elements
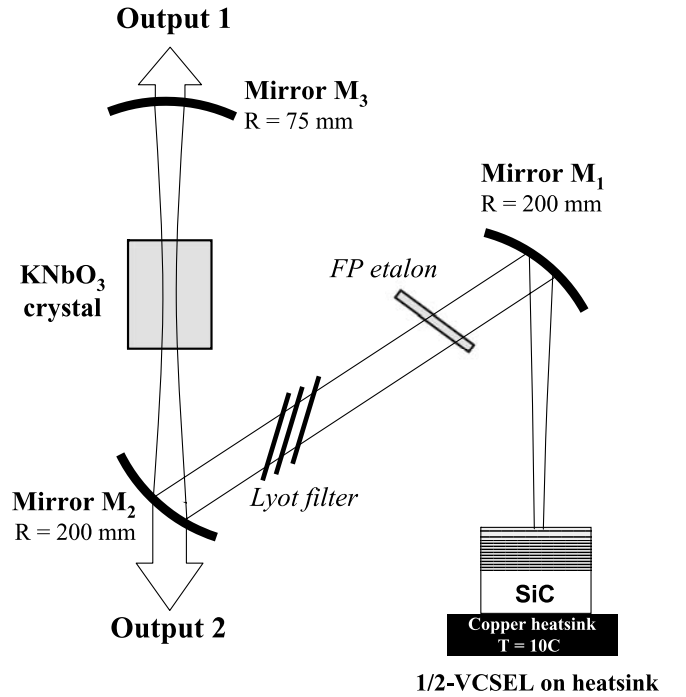

FIGURE 11 Experimental set-up achieved for the second harmonic generation process at 501.7 nm in a four-mirror cavity with the Lyot filter, the etalon and the KNbO$_3$ doubling crystal

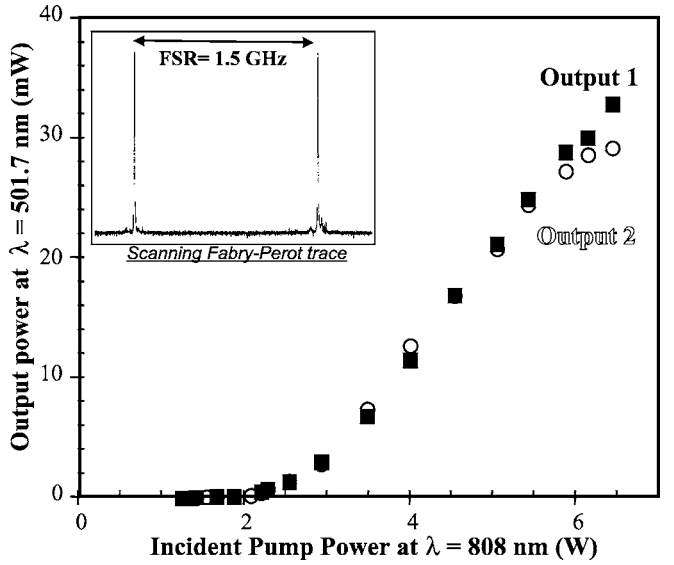**FIGURE 12** cw laser output power at $\lambda = 501.7$ nm vs. the incident pump power for a 75.6 °C temperature of the non-linear crystal. The *inset* shows the frequency spectrum obtained with the scanning Fabry–Pérot interferometer confirming single-frequency operation

and the mirrors also reduce the intracavity infrared laser power. The frequency spectrum of the fundamental infrared laser beam was also analysed with the same Fabry–Pérot interferometer as explained previously. The inset of Fig. 12 is a typical scanning trace, which demonstrates the single-frequency operation of the laser with a SMSR higher than 20 dB.

Although these results are preliminary and the second harmonic generation process is not yet fully optimised, they represent, to the best of our knowledge, the high-

est single-frequency laser power obtained by intracavity SHG of a VECSEL ever reported in literature. Moreover, the single frequency output power at 501.7 nm is similar to that obtained with an Yb-doped laser crystal and a $KNbO_3$ frequency-doubling crystal as in [19]. Here we take the benefit of a much simpler design of the laser cavity to control the laser wavelength and force single-frequency operation.

7 Conclusion

In this work we report a complete theoretical and experimental study of the operation of a high-power diode-pumped VECSEL at 1003 nm, and 501 nm by intracavity second-harmonic generation. Thanks to an original technique based on the $AuIn_2$ solid-liquid inter-diffusion bonding, the active structure had been bonded onto a SiC substrate exhibiting a low thermal impedance. This technical procedure should also be applied to bonding onto a diamond substrate for an even lower thermal resistance. We then obtained a maximum output power of 1.7 W in a simple and compact plano-concave cavity, limited by the available incident pump power. The improvement of the thermal dissipation from the active region has been experimentally checked with both laser characterisations and temperature mappings under high power optical pumping. It was theoretically explained through the evaluation of the thermal resistance of the 1/2-VCSEL, which allows us to predict the conditions for optimal laser operation.

With the insertion of only a solid Fabry–Pérot etalon it has been possible to pick the emission wavelength at 1003 nm and to force a single-frequency operation with up to 500 mW of output power. A simple model has been used to explain that laser emission on a single longitudinal mode is possible even with our low finesse and large FSR etalon. We further demonstrate that, due to the multimode nature of the optical pump source used, an intracavity filter is necessary to develop high power single-frequency VECSEL systems. Finally, motivated by the interest of blue-green single-frequency emission around 501.7 nm for metrological applications such as iodine-based laser stabilisation, second harmonic generation has been performed with a $KNbO_3$ nonlinear crystal. A maximum visible power of 62 mW has been generated in a four-mirror Z-cavity, which compare favourably with those obtained with bulk ytterbium-doped crystals. At both wavelengths (1003 nm and 501.7 nm), these results repre-

sent the highest single-frequency power ever reported from a VECSEL.

REFERENCES

1 M. Kuznetsov, F. Hakimi, R. Sprague, A. Mooradian, IEEE J. Sel. Top. Quantum Electron. **5**, 561 (1999)
2 W.J. Alford, T.D. Raymond, A.A. Allerman, J. Opt. Soc. Am. B **19**, 663 (2002)
3 S. Hoogland, S. Dhanjal, A. Tropper, J. Roberts, R. Häring, R. Paschotta, F. Morier-Genoud, U. Keller, IEEE Photon. Technol. Lett. **12**, 1135 (2000)
4 A. Garnache, S. Hoogland, A. Tropper, I. Sagnes, G. Saint-Girons, J. Roberts, Appl. Phys. Lett. **80**, 3892 (2002)
5 A. Garnache, A. Kachanov, F. Stoeckel, R. Houdre, J. Opt. Soc. Am. B **7**, 1589 (2000)
6 M. Holm, D. Burns, A. Ferguson, A. Ferguson, M. Dawson, IEEE Photon. Technol. Lett. **11**, 1551 (1999)
7 R.H. Abram, K.S. Gardner, E. Riis, A.I. Ferguson, Opt. Express **12**, 5434 (2004)
8 A. Ouvrard, A. Garnache, L. Cerutti, F. Genty, D. Romanini, IEEE Photon. Technol. Lett. **17**, 2020 (2005)
9 J.E. Hastie, J.M. Hopkins, S. Calvez, C.W. Jeon, D. Burns, R.H. Abram, E. Riis, A.I. Ferguson, M.D. Dawson, IEEE Photon. Technol. Lett. **13**, 894 (2003)
10 S. Lutgen, T. Albrecht, P. Brick, W. Reill, J. Luft, W. Späth, Appl. Phys. Lett. **82**, 3620 (2003)
11 J. Chilla, S. Butterworth, A. Zeitschel, J. Charles, A. Caprara, M. Reed, L. Spinelli, Proc. SPIE **5332**, 143 (2004)
12 K.S. Kim, J.R. Yoo, S.H. Cho, S.M. Lee, S.J. Lim, J.Y. Kim, J.H. Lee, T. Kim, Y.J. Park, Appl. Phys. Lett. **88**, 091 107 (2006)
13 J. Dion, I. Sagnes, M. Strassner, State-of-the-Art Program on Compound Semiconductors XLI (2004)
14 F. Du Burck, C. Daussy, A. Amy-Klein, A. Goncharov, O. Lopez, C. Chardonnet, IEEE J. Trans. Instrum. Meas. **54**, 754 (2005)
15 J.L. Hall, L.-S. Ma, M. Taubman, B. Tiemann, F.-L. Hong, O. Pfister, J. Ye, IEEE J. Trans. Instrum. Meas. **48**, 583 (1999)
16 W.Y. Cheng, L. Chen, T.H. Yoon, J.L. Hall, Y. Ye, Opt. Lett. **27**, 571 (2002)
17 J.-C. Keller, M. Broyer, J.-C. Lehmann , CR. Acad. Sci. Paris, tome 277-série B, **369** (1973)
18 J. Ye, L.S. Ma, J.L. Hall, J. Opt. Soc. Am. B **17**, 927 (2000)
19 M. Jacquemet, F. Druon, F. Balembois, P. Georges, B. Ferrand, Opt. Express **13**, 2345 (2005)
20 L. Fan, T.-C. Hsu, M. Fallahi, J. Murray, R. Bedford, Y. Kaneda, J. Hader, A. Zakharian, J. Moloney, S. Koch, W. Stolz, Appl. Phys. Lett. **88**, 251 117 (2006)
21 L.A. Coldren, S.W. Morzine, *Diode Lasers and Photonic Integrated Circuits* (Wiley, New York, 1995)
22 M. Jacquemet, M. Domenech, J. Dion, M. Strassner, G. Lucas-Leclin, P. Georges, I. Sagnes, A. Garnache, Proc. SPIE **6184**, 61 841X (2006)
23 M. Reichling, H. Grönbeck, J. Appl. Phys. **75**, 1914 (1994)
24 A. Garnache, A. Ouvrard, D. Romanini, Proc. CLEO Europe 2005, paper CB19
25 S. Chénais, S. Forget, F. Druon, F. Balembois, P. Georges, Appl. Phys. B **79**, 221 (2004)